THE APPLICATION OF THE NEARLY OPTIMAL SPONGE BOUNDARY CONDITIONS FOR SEISMIC WAVE PROPAGATION IN POROELASTIC MEDIA

JINGYI CHEN[1*], RALPH PHILLIP BORDING[1], ENRU LIU[2], ZHONGJIE ZHANG[3] and JOSÉ BADAL[4]

[1] *Department of Earth Sciences, Memorial University of Newfoundland, St. John's, Newfoundland, Canada A1B 3X5. jingyi-chen@utulsa.edu, pbording@mun.ca*
[2] *ExxonMobil Upstream Research Company, Geophysics Division, Houston, TX 77252-2189, U.S.A. enru.liu@exxonmobil.com*
[3] *State Key Laboratory of Lithosphere Evolution, Institute of Geology and Geophysics, Chinese Academy of Sciences, Beijing, 100029, China. zhangzj@mail.iggcas.ac.cn*
[4] *Physics of the Earth, Sciences B, University of Zaragoza, Pedro Cerbuna 12, 50009 Zaragoza, Spain. badal@unizar.es*
[*] *Present address: Dept. of Geosciences, The University of Tulsa, Keplinger Hall, 441 South Gary, Tulsa, OK 74104, U.S.A.*

(Received March 12, 2009; revised version accepted September 27, 2009)

ABSTRACT

Chen, J., Bording, J.P., Liu, E., Zhang, Z. and Badal, J., 2010. The application of the nearly optimal sponge boundary conditions for seismic wave propagation in poroelastic media. *Journal of Seismic Exploration*, 19: 1-19.

Absorbing boundary conditions (ABC) play an important role in eliminating artificial reflections from the edges of the seismic model. In this paper, we present a modified nearly optimal sponge boundary condition. Utilizing the measure of reflected wave energy it is possible to construct a contour map for a range of sponge absorption coefficients and numbers of grid points at tapered zone, and determine the best set of parameters to minimize this energy metric. We apply this optimal scheme to the numerical simulation of seismic wave propagation in 2D transversely isotropic poroelastic media using staggered-grid finite-difference operator. We consider a first-order hyperbolic system that is equivalent to Biot/squirt equation. The vector of unknowns in this system consists of the solid and fluid particle velocity components, the solid stress components and the fluid pressure. Eighth-order accuracy in space and second-order accuracy in time are used in our numerical computation. Modeling studies indicate remarkably good results, the nearly optimal sponge boundary conditions is simple and effective enough to eliminate the artificial reflections from the boundaries of the model.

KEYWORDS: boundary conditions, numerical modeling, poroelastic media, Biot/squirt mechanism, staggered-grid finite-difference.

0963-0651/10/$5.00

INTRODUCTION

Seismic numerical simulation is an effective method to help us understand the elastic seismic wave responses (e.g., amplitude, frequency, attenuation, and dispersion) for different environments of reservoir rocks. However, for the limitation of the computational domain, we often treat seismic waves propagation in truncated domain with boundaries. Thus, One of the tough problems arises in application of seismic numerical modeling is the presence of reflections from the edges of the seismic model (Cerjan et al., 1985). These undesired events eventually override the actual seismic signals that propagate in the modeled region.

During the last 30 years, numerous techniques have been developed for dealing with the problem of existing artificial reflections mentioned above: absorbing layers and absorbing boundary conditions (ABC). In the context of absorbing layers, Bérenger (1994) introduced a technique called the perfectly matched layer (PML) that has the remarkable property of generating no reflection at the interface between the free medium and the artificial absorbing medium. This method has been proven to be more efficient and has become widely used. Another approach to improve PML absorbing behavior has been developed for Maxwell's equations by Kuzuoglu and Mittra (1996) and Roden and Gedney (2000) and named convolutional-PML (C-PML). Komatitsch and Martin (2007) further improved this technique to unsplit C-PML. In the C-PML it is only necessary to store the memory variables in the absorbing strips, and its cost in terms of memory storage is similar to that of the classical PML (Komatitsch and Martin, 2007). All numerical results (Komatitsch and Martin, 2007; Martin et al., 2008) demonstrated the efficiency of this improved C-PML.

Absorbing boundary conditions (ABC) are an alternative to absorbing layers. Many authors introduced various boundary conditions in numerical modeling, for instance, paraxial conditions (Clayton and Engquist, 1977; Higdon, 1991; Quarteroni et al., 1998), the eigenvalue decomposition method (Dong et al., 2005), continued fraction absorbing boundary conditions(Guddati and Lim, 2006). Cerjan et al. (1985) introduced sponge boundary condition specified an operator length (grid points at tapered zone) and absorption coefficient for the exponential weight, this boundary condition is commonly used in seismic numerical modeling because of its simplicity and validity. The heuristic given by Cerjan uses a zone of 20 grid points and an exponential weight based on an initial value of 0.015 (Bording, 2004). What are the values (operator length and absorption coefficient) to use in given problems? Or how to use these values effectively. Bording's paper (Bording, 2004) further discussed its effect in acoustic media by minimizing wavefield energy and optimizing the parameters of absorption coefficient and the width of tapered zone. Here, we will apply modified Bording's method to the numerical modeling

of seismic wave propagation in the transversely isotropic poroelastic media based on Biot/squirt flow theory.

The Biot theory (Biot, 1956a,b, 1962) has long been regarded as a basis for solving wave-propagation problems in fluid-filled porous media. Biot's mechanism is responsible for the observed values of attenuation in reservoir rocks at seismic frequencies (Carcione, 2007). Many papers discussed the proper uses of the Biot's theory (White, 1975; Carcione et al., 2003; Pride et al., 2004; Carcione and Picotti, 2006). Many investigators have shown that the squirt-flow mechanism can be responsible for the observed large attenuation and velocity dispersion (Dvorkin et al., 1994; Yang and Zhang, 2000, 2002). A consistent theory dealing simultaneously with Biot and squirt-flow (BISQ) mechanisms has been presented by Dvorkin and Nur (1993). The theory includes those mechanisms by considering the fluid motion parallel (the Biot mechanism) and transverse (the squirt-flow mechanism) to direction of a planar P-wave. Many authors have made contributions on Biot/squirt theory and applications. Parra (1997) extended this BISQ theory to frequency domain include the transversely isotropic poroelastic medium. Yang and Zhang (2000, 2002) developed a generalized poroelastic equation to relate wave propagation with the solid/fluid coupling anisotropy and both mechanisms. Although it is known now that the squirt-flow mechanism has no influence in the seismic and sonic bands (Pride et al, 2004), we still use the BISQ theory in this paper based on mainly discussing the application of boundary conditions in the complex poroelastic media.

Regarding the numerical modeling, the finite-difference method has been used to simulate wave propagation in poroacoustic media by Hassanzadeh (1991) and in heterogeneous poroelastic media by Dai et al. (1995). Biot's equations in anisotropic media have been solved numerically by Carcione (1996). The poro-viscoelastic case has been discussed in Carcione (1998) including the BISQ and in Carcione and Helle (1999). Because central finite-difference operators for the first derivatives are less accurate than staggered-grid finite-difference operators, many authors have used staggered operators to simulate seismic wave propagation (Faria and Stoffa, 1994; Carcione, 1998; Carcione and Helle, 1999; Moczo et al., 2000; Zeng and Liu, 2001; Mittet, 2002; Sheen et al., 2006).

In this paper, we apply the modified Bording's absorbing boundary condition to eliminate artificial reflections from the boundaries of the numerical model. Biot/Squirt equations (Biot, 1956a, b, 1962, Yang and Zhang, 2000, 2002) are reformulated into a first-order system whose vector of unknowns consists of the solid and fluid particle velocity components, the solid stress components, and the fluid pressure. For the implementation of the staggered-grid finite-difference method, eighth-order accuracy in space and

second-order accuracy in time are used, and a harmonic average scheme is applied for effective media parameters. The results of modeling test show us that this method is effective to eliminate the reflections from the edges of model after using the optimal operator length and absorption coefficient.

BIOT/SQUIRT MECHANISM

Yang and Zhang (2000, 2002) extend the Biot/squirt (BISQ) theory to include the solid/fluid coupling anisotropy and develop a general 3D poroelastic wave equation in time domain including both mechanisms simultaneously.

$$\sum_{j=1}^{3} (\partial \tau_{ij} / \partial x_j) = (\partial^2/\partial t^2)(\rho u_i + \rho_f w_i) \quad , \tag{1}$$

$$-(\partial P/\partial x_i) = (\partial^2/\partial t^2)(\rho_f u_i + m_{ii} w_i) + (\eta/\kappa_{ii})(\partial w_i/\partial t) \quad , \tag{2}$$

where i,j = 1,2,3. The parameters describing the physical properties of the medium are defined as follows:

τ_{ij} denotes the total stress component of the bulk material; u_i is the displacement component for solid; $w_i = \phi(U_i - u_i)$ represents the displacement component for the fluid relative to that for the solid; U_i is the displacement component for fluid; ϕ is the porosity; ρ is the overall density of the saturated media determined by $\rho_1 + \rho_2$, $\rho_1 = (1 - \phi)\rho_s$ and $\rho_2 = \phi\rho_f$; ρ_f and ρ_s are the density of the fluid and the solid, respectively; P denotes fluid pressure; η represents the viscosity of the pore fluid; m_{ii} denotes the component of coefficient constant introduced initially by Biot (1962); κ_{ii} denotes the permeability of the matrix, these two are 3 × 3 diagonal matrixes.

The expression of the stress-strain relation in terms of the effective stress or total stress is defined as

$$\tau = Ae - \alpha P \quad , \tag{3}$$

where $\tau = (\tau_{ij})$ indicates the total stress tensor of the saturated porous medium, A denotes the solid-frame stiffness tensor containing 21 independent drained elastic coefficients for general anisotropic media, $\alpha = (\alpha_{ij})$ is the poroelastic coefficient tensor of the effective stress, $e = (e_{ij})$ represents the strain tensor of the porous medium, $e_{ij} = \frac{1}{2}[(\partial u_i/\partial x_j) + (\partial u_j/\partial x_i)$, i,j = 1,2,3.

We can also get the expression of fluid pressure P in 3D,

$$P = \sum_{i=1}^{3} F_i S_i [(\partial U_i / \partial x_i) + \{(\alpha_{ii} - \phi)/\phi\} e_{ii} + \sum_{\substack{j=1 \\ j \neq i}}^{3} (\alpha_{ii}/\phi) e_{ij}] \quad , \tag{4}$$

where F_i and S_i are the Biot-flow coefficient and the characteristic squirt-flow coefficient, respectively. The two coefficients are defined by the following equations:

$$1/F_j = 1/K_f + [\sum_{i=1}^{3} (\alpha_{ij} - \phi)]/\phi K_s] \quad ,$$

$$S_j(\omega) = 1 - 2J_1(\gamma_j R_j)/\gamma_j R_j J_0(\gamma_j R_j) \quad ,$$

$$\gamma_j^2 = (\rho_f \omega^2 / F_j)[(\beta \rho_f + \phi m_j)/\rho_f + i(\omega_j/\omega)] \quad ,$$

$$\omega_j = (\eta \phi / 2\rho_f) \sum_{\substack{i,k=1 \\ i \neq j}}^{3} \beta_{kj} r_{ik} \quad ,$$

$$m_j = \tfrac{1}{2} \sum_{\substack{i,k=1 \\ i \neq j}}^{3} \beta_{kj} m_{ik} \quad ,$$

$$\beta_{kj} = \begin{cases} \beta & , \quad j = k \\ 1 - \beta & , \quad j \neq k \end{cases}$$

$$r_{ik} = 1/\kappa_{ik} \quad , \quad i,j,k = 1,2,3$$

where K_f and K_s are the bulk moduli of the pore fluid and solid material, respectively, K_f is set by $V_{pf} = \sqrt{(K_f/\rho_f)}$, V_{pf} is the acoustic velocity of the fluid, J_0 and J_1 are the Bessel functions of zero-order and first-order, respectively, the parameter R_j represents the average characteristic squirt-flow length of fluids squirting in the j-th direction, the parameter β indicates the ratio of the transversely average displacement of solid to that of the fluid, r_{ik} is the vector of fluid impedance.

Considering the simple anisotropy situation, 2D (xz-plane) wave propagation in the transversely isotropic media with a horizontal symmetry axis (HTI). Eqs. (1)-(4) can be written as a set of first-order hyperbolic differential equations in time domain for v, V, τ and P:

$$\partial v_x/\partial t = A_{11}\phi m_{11}[(\partial \tau_{xx}/\partial x) + (\partial \tau_{xz}/\partial z)] + A_{11}\rho_2(\partial P/\partial x) + A_{11}b_{11}\rho_2(V_x - v_x) \quad , \tag{5a}$$

$$\partial V_x/\partial t = -A_{11}(\rho_f - \phi m_{11})[(\partial \tau_{xx}/\partial x) + (\partial \tau_{xz}/\partial z)] - A_{11}\rho_1(\partial P/\partial x) - A_{11}b_{11}\rho_1(V_x - v_x) \quad , \tag{5b}$$

$$\partial v_z/\partial t = A_{33}\phi m_{33}[(\partial \tau_{xz}/\partial x) + (\partial \tau_{zz}/\partial z)] + A_{33}\rho_2(\partial P/\partial z) + A_{33}b_{33}\rho_2(V_z - v_z) \quad , \tag{5c}$$

$$\partial V_z/\partial t = -A_{33}(\rho_f - \phi m_{33})[(\partial \tau_{xz}/\partial x) + (\partial \tau_{zz}/\partial z)] - A_{33}\rho_1(\partial P/\partial z) - A_{33}b_{33}\rho_1(V_z - v_z) \quad , \tag{5d}$$

$$\partial \tau_{xx}/\partial t = C_{11}(\partial v_x/\partial x) + C_{13}(\partial v_z/\partial z) - \alpha_{11}(\partial P/\partial t) \quad , \tag{5e}$$

$$\partial \tau_{zz}/\partial t = C_{31}(\partial v_x/\partial x) + C_{33}(\partial v_z/\partial z) - \alpha_{33}(\partial P/\partial t) \quad , \tag{5f}$$

$$\partial \tau_{xz}/\partial t = C_{55}[(\partial v_z/\partial x) + (\partial v_x/\partial z)]/2 \quad , \tag{5g}$$

$$\partial P/\partial t = -F_1S_1[(\partial V_x/\partial x) + (\{\alpha_{11} - \phi\}/\phi)(\partial v_x/\partial x)] - F_3S_3[(\partial V_z/\partial z) + (\{\alpha_{33} - \phi\}/\phi)(\partial v_z/\partial z)] \quad , \tag{5h}$$

where $v_x = \partial u_x/\partial t$, $v_z = \partial u_z/\partial t$, $V_x = \partial U_x/\partial t$, $V_z = \partial U_z/\partial t$, $A_{ii} = 1/[\rho_1\phi m_{ii} - \rho_2(\rho_f - \phi m_{ii})]$, $b_{ii} = \eta\phi/\kappa_{ii}$, $\kappa_{ii} = 1/r_{ii}$ is the permeability vector of porous media, $i = 1,3$, C_{11}, C_{13}, C_{31}, C_{33} and C_{55} are elastic coefficients of solid media, $\alpha_{11} = 1 - (C_{11} + 2C_{13})/3K_s$, $\alpha_{33} = 1 - (C_{13} + C_{23} + C_{33})/3K_s$, $m_{11} = (\phi\rho_f + \rho_{ax})/\phi^2$, $m_{33} = (\phi\rho_f + \rho_{az})/\phi^2$, ρ_{ax} and ρ_{az} are the additional coupling densities along the x- and z-directions in the system of Cartesian coordinates.

FINITE-DIFFERENCE IMPLEMENTATION

The system of eq. (5) is easily solved using a staggered-grid finite-difference technique (Virieux, 1986; Levander, 1988; Graves, 1996; Moczo et al., 2000). Details of this type of formulation can be found in the above articles, along with numerical accuracy and stability analyses. Because the item S_i is frequency-dependent, we deal with this in the time domain by considering it as quasi-constant during numerical computation. Fig. 1 illustrates the layout of the wavefield variables and media parameters on the staggered-grid mesh. One of the attractive features of the staggered-grid approach is that the various

difference operators are all naturally centered at the same point in space and time.

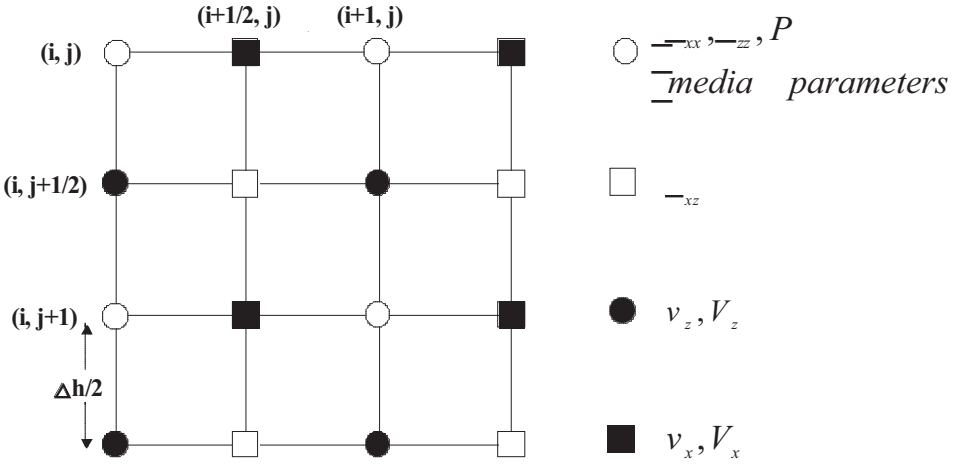

Fig. 1. Grid layout for staggered-grid formulation. Indices (i,j) represent spatial coordinates (x,z), respectively, and grid spacing $\Delta h = \Delta x = \Delta z$ is defined as a length between centers of two adjacent grid cells.

In the above equations, the superscripts denote the time step, and the subscripts denote the spatial indices. The symbol L_x and L_z represents the discrete form of the spatial differential operator along x- and z-coordinates direction, for 2L-order accuracy along the x-direction as example,

$$L_x u|_{i,j} = (1/\Delta x) \sum_{m=1}^{L} a_m (u_{i+(2m-1)/2,j} - u_{i-(2m-1)/2,j}) \quad , \tag{7}$$

and the differential coefficient (Mou and Pei, 2005)

$$a_m = (-1)^{m+1} \prod_{i=1, i\neq m}^{L} (2i-1)^2/(2m-1) \prod_{i=1}^{L-1} [(2m-1)^2 - (2i-1)^2] \quad ,$$

where Δx is grid spacing, and $\Delta x = \Delta z$ in this paper. $\bar{V}$ denotes the arithmetic average in time domain, $(V^{n+1/2} + V^{n-1/2})/2$, and the coefficients A_x, B_x, C_x, D_x, E_x and F_x are defined as

$$A_x = \underline{A}_{11x} \underline{b}_{11x} \underline{\rho}_{2x} \quad ,$$

$$B_x = \underline{A}_{11x} \underline{\phi}_x \underline{m}_{11x} \quad ,$$

$$C_x = \underline{A}_{11x} \underline{\rho}_{2x} \quad ,$$

$$D_x = \underline{A}_{11x} (\underline{\rho}_{fx} - \underline{\phi}_x \underline{m}_{11x}) \quad ,$$

$$E_x = \underline{A}_{11x} \underline{\rho}_{1x} \quad ,$$

$$F_x = \underline{A}_{11x} \underline{b}_{11x} \underline{\rho}_{1x} \quad .$$

The effective media parameters yield a more accurate representation in the region near interfaces (Zahradnik et al., 1993; Graves, 1996). The parameters are given by the harmonic average:

$$\begin{aligned} \underline{\rho}_{fx} &= [1/2\{(1/\rho_{f_{i,j}}) + (1/\rho_{f_{i+1,j}})\}]^{-1} \quad , \\ \underline{\rho}_{fz} &= [1/2\{(1/\rho_{f_{i,j}}) + (1/\rho_{f_{i,j+1}})\}]^{-1} \quad , \end{aligned} \tag{8}$$

for the fluid density in porous media. Similar averages are applied for other media parameters, like A_{11}, A_{33}, b_{11}, b_{33} and ρ_s. The anisotropic elastic parameters are obtained by

$$\underline{C} = [1/4\{(1/C_{i,j}) + (1/C_{i+1,j}) + (1/C_{i,j+1}) + (1/C_{i+1,j+1})\}]^{-1} \quad , \tag{9}$$

this harmonic averaging scheme is effective for simulating seismic wave propagation in heterogeneous media (Moczo et al. , 2002).

NEARLY OPTIMAL ABSORBING BOUNDARY CONDITIONS

Sponge absorbing boundary conditions (Sochacki et al., 1987; Cerjan, 1985; Bording, 2004) is the commonly used technique in numerical modeling to eliminate the artificial reflections from boundaries of the model. It is based on the gradual reduction of wave amplitudes in the vicinity of artificial boundaries. This reduction is tapered gradually by the use of a weighting function W(x,z) of the form

$$W(x,z) = \begin{cases} \exp-[a(b-x)]^2 & , \ x < b \text{ or } x > L_x - b \\ \exp-[a(b-z)]^2 & , \ z < b \text{ or } x > L_z - b \\ 1 & \text{elsewhere} \end{cases} , \qquad (10)$$

where a is the absorption coefficient, b is the width of tapered zone, and L_x and L_z are the model sizes of the x- and z-direction.

Cerjan (1985) specified the above operator length b and absorption coefficient a for the exponential weight. These variables are dependent on the wave equation formulation and numerical implementation. Bording (2004) developed and presented an energy metric to obtain the optimal parameters of absorbing boundary condition, in fact, the similar method of minimizing the amount of energy had been introduced in an earlier paper by Collino and Monk (1998). However, only one-way acoustic equation was adopted in Bording's paper, and determining the best set of unknown parameters to minimize the energy of the whole wave field. We know that the media in the earth are complex and anisotropic, the velocities along different directions of seismic wave propagation are different. Especially, they are more challenging in poroelastic media, the seismic waves propagating in this kind of media will become more complex including fast and slow quasi-compressional waves, quasi-shear wave, even wave scatters. Clearly, this optimal scheme has some limitations to poroelastic media. For simplicity, we divide the whole wave field into two domains (Fig. 2), one is along the x-direction, another is along the z-direction. To determine the best parameters for this implementation, the operator length and absorption coefficient are varied over a range of values. We sum up all energies of all reflections from boundaries and determine the best set of parameters to minimize this energy metric along the two directions based on grids, respectively. Fig. 2 gives three lines (x1, x2, x3; z1, z2, z3) along x- and z-directions, respectively, these lines cover ranges of reflections from small angles to the vertical angle.

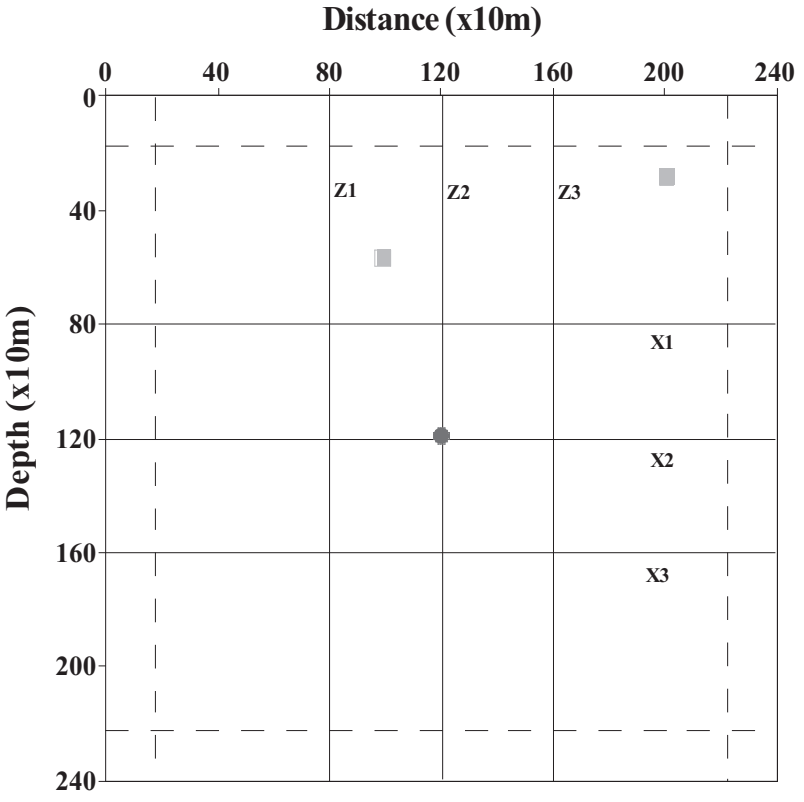

Fig. 2. The configuration of the measured lines. The solid lines represent the measured lines, and the zones between dash lines and model boundaries denote the tapered zone. The solid circle indicates the source position, and the solid squares indicate the receivers.

SOURCE IMPLEMENTATION

The source time function used in this paper is a band-limited Ricker wavelet (Lou and Rial, 1995), which is distributed over a small region of the grid, that is:

$$f(t,x,z) = \lfloor 1 - 2\pi^2 f^2 (t - t_0)^2 \rfloor \exp \lfloor -\pi^2 f^2 (t - t_0)^2 \rfloor$$
$$\exp\{-\lambda \lfloor (x - x_0)^2 + (z - z_0)^2 \rfloor\} \quad , \qquad (11)$$

where t_0 is the original time of the source function, f is the dominant frequency of the source, x_0 and z_0 are the central position of source, and λ determines the degree of concentration of the source function. In this study, we choose t_0 = 0.05 s, f = 25 Hz, λ = 0.1 as a common source signal in modeling seismic exploration.

NUMERICAL TEST

In our water-saturated model, we select Taylor sandstone as solid HTI media (Sedimentary rock) based on data from Thomsen (1986). Measured anisotropic parameters are available in Table 1, then we use following equations to get the elastic coefficients of the HTI media:

$$C_{33} = V_{P0}^2\rho, \quad C_{44} = V_{S0}^2\rho, \quad C_{11} = C_{33} + 2C_{33}\epsilon, \quad C_{66} = C_{44} + 2\gamma C_{44},$$

$$C_{13} = \sqrt{\{(C_{33} - C_{44})^2 + 2C_{33}(C_{33} - C_{44})\delta\}} - C_{44},$$

Table 1. Measured anisotropic parameters of Taylor sandstone (Thomsen, 1986).

Sample	V_P (m/s)	V_S (m/s)	ϵ	δ	γ	ρ (g/cm^3)
Taylor sandstone	3368	1829	0.110	−0.035	0.255	2.500

Table 2. All physical properties (rock and fluid) of Taylor sandstone used in two examples.

Properties	Solid	Fluid	
	Taylor sandstone	Water	Gas
V_P (m/s)	3368	1500	630
V_S (m/s)	1829	-	-
ρ (g/cm^3)	2.500	1.000	0.140
ρ_{ax},ρ_{az} (g/cm^3)	0.300, 0.33	-	-
ϕ (%)	19	-	-
K_S (Pa)	12.402E+9	-	-
η (Pa * s)	-	1.000E-3	2.200E-5
β		0.4	
k_{11},k_{33} (md)	100,100	-	-
R_x,R_z (mm)	-	5, 5	5, 5

(a)

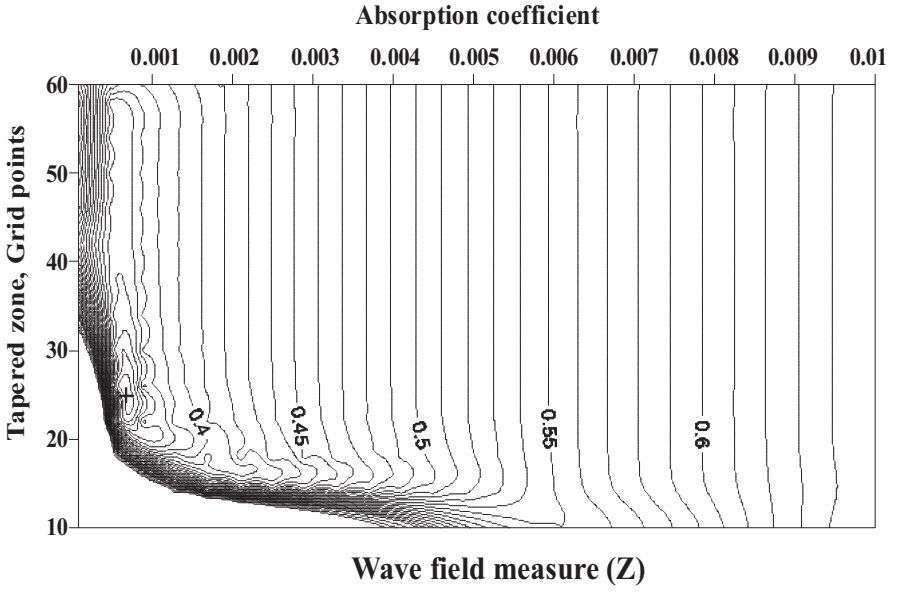

(b)

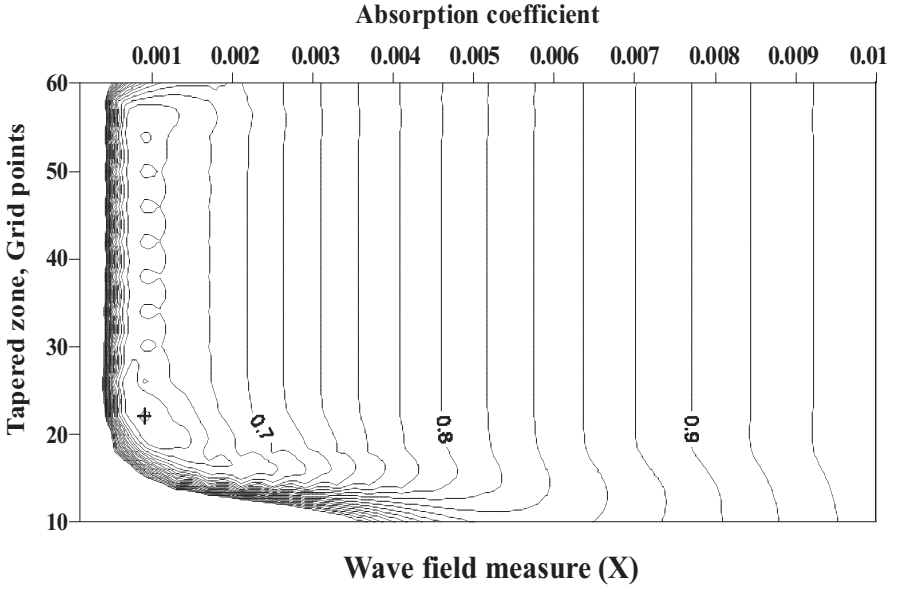

Fig. 3. Wavefield energy contour plot of tapered zone grid points versus absorption coefficient. (a) denotes energy measurement along z-direction, (b) represents energy measurement along x-direction. The cross symbols denote the optimal parameters.

where V_{P0}, V_{S0} are vertical velocities of the P-wave and S-wave in anisotropic media, respectively, ϵ, δ and γ are Thomsen's anisotropic parameters, Thomsen (1986) provides the detailed description, in addition, the elastic coefficients have some features in HTI media, $C_{22} = C_{33}$, $C_{55} = C_{66}$ and $C_{23} = C_{22} - 2C_{44}$. All the physical properties of the Taylor sandstone used in the model are given in Table 2.

The size of the model with water-saturated porous media is $N_x \times N_z = 240 \times 240$ nodes. The spatial grid spacings are 10 m and 10 m whereas the time step is 1 ms. The explosive source with 25 Hz of dominant frequency is located at the center-grid position of the model, the red sold circle indicates the source position in Fig. 2. When seismic wave propagates 360 ms after the source is generated, we compute the total energies of reflections from boundaries along x- and z-directions, respectively. In Fig. 2, the solid lines represent the measured lines, and the zones between the dashed lines and the model boundaries denote the tapered zone. The contour plot of the energy metric shown in Fig. 3; Fig. 3a denotes the measurement of the wave field energy along the z-direction, Fig. 3b denotes the x-direction. The cross symbol denotes the optimal parameters, Fig. 3 clearly indicates an optimal operator length and absorption coefficient at 25 and 0.0007 along the z-direction, 22 and 0.0009 along the x-direction. To compare the effectiveness of the absorbing boundary condition, two cases of the model were run, one without the sponge boundary applied, and another with the optimal parameters, shown in Figs. 4 and 5 at the snapshots time 360 ms, respectively. In Figs. 4 and 5, (a) and (b) are the horizontal and vertical components of the solid particle velocity, respectively, (c) and (d) are the horizontal and vertical components of the fluid particle velocity, respectively. Fig. 5 indicates our modified boundary condition is extremely effective to eliminate the reflections from boundaries. In these diagrams, the wave type is indexed as qP or qS_v for a quasi-compressional or a quasi-shear wave; a superscript is used for the phase velocity, for fast and for slow.

To test our nearly optimal boundary condition, we also compare with the C-PML boundary condition and the exact solution as described in Komatitsch and Martin (2007). Fig. 6 illustrates the seismograms (the recording time is 470ms) at the receiver position (60,100) as the green solid square indicates nongrazing incidence, where the grid number is 60 along the z-direction, 100 along the x-direction. Fig. 6a shows the horizontal component of the solid velocity. Fig. 6b shows the vertical component of the solid velocity. Fig. 6c shows the horizontal component of the fluid velocity. Fig. 6d shows the vertical component of the fluid velocity. Fig. 7 illustrates the seismograms (the recording time is 470 ms) at the receiver position (30,200) as another green solid square indicates grazing incidence. Fig. 7a shows the horizontal component of the solid velocity. Fig. 7b shows the vertical component of the solid velocity. Fig. 7c shows the horizontal component of the fluid velocity.

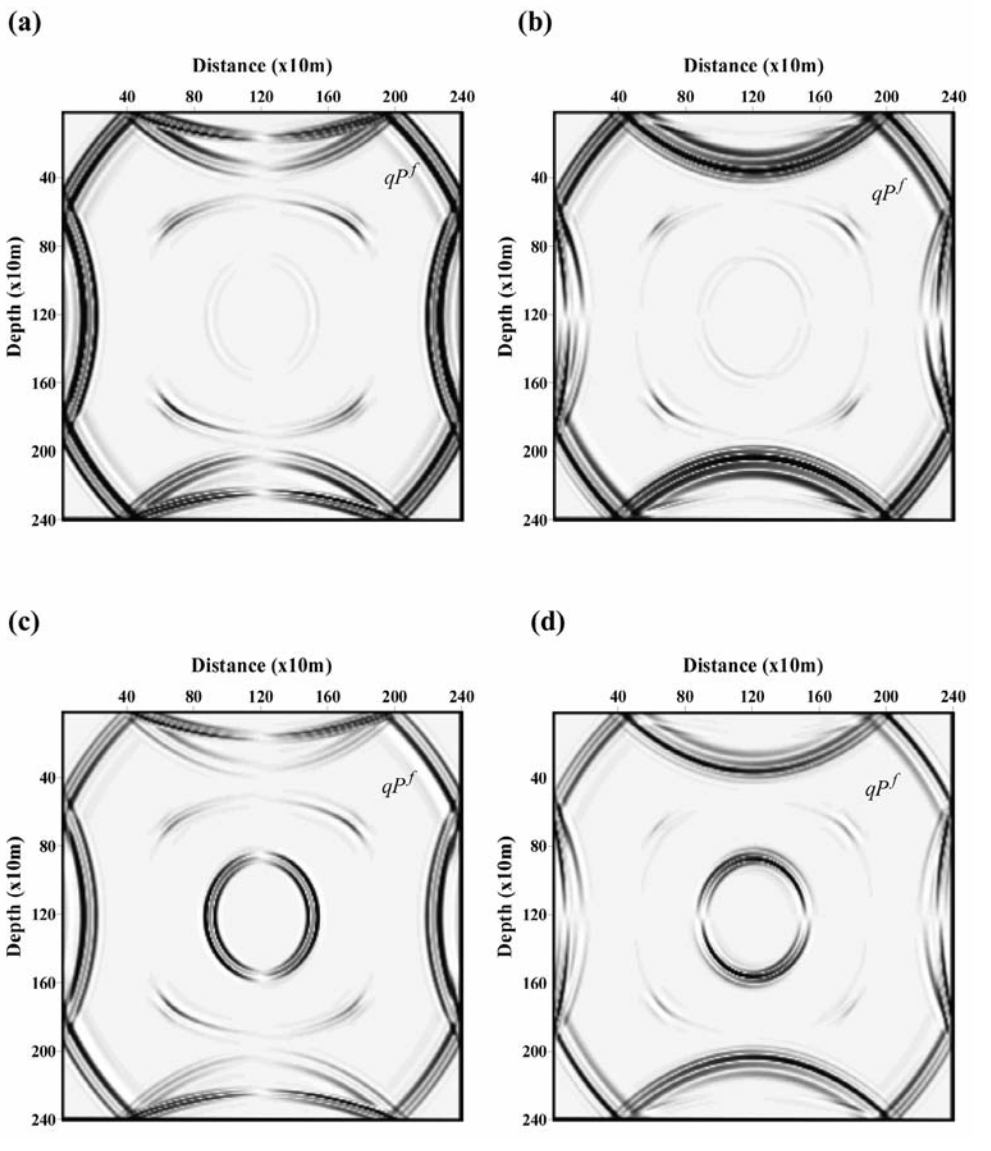

Fig. 4. Snapshots (t = 360 ms) of the horizontal (a,c) and vertical (b,d) components for the solid and fluid particle velocities based on BISQ mechanism without applying boundary conditions.

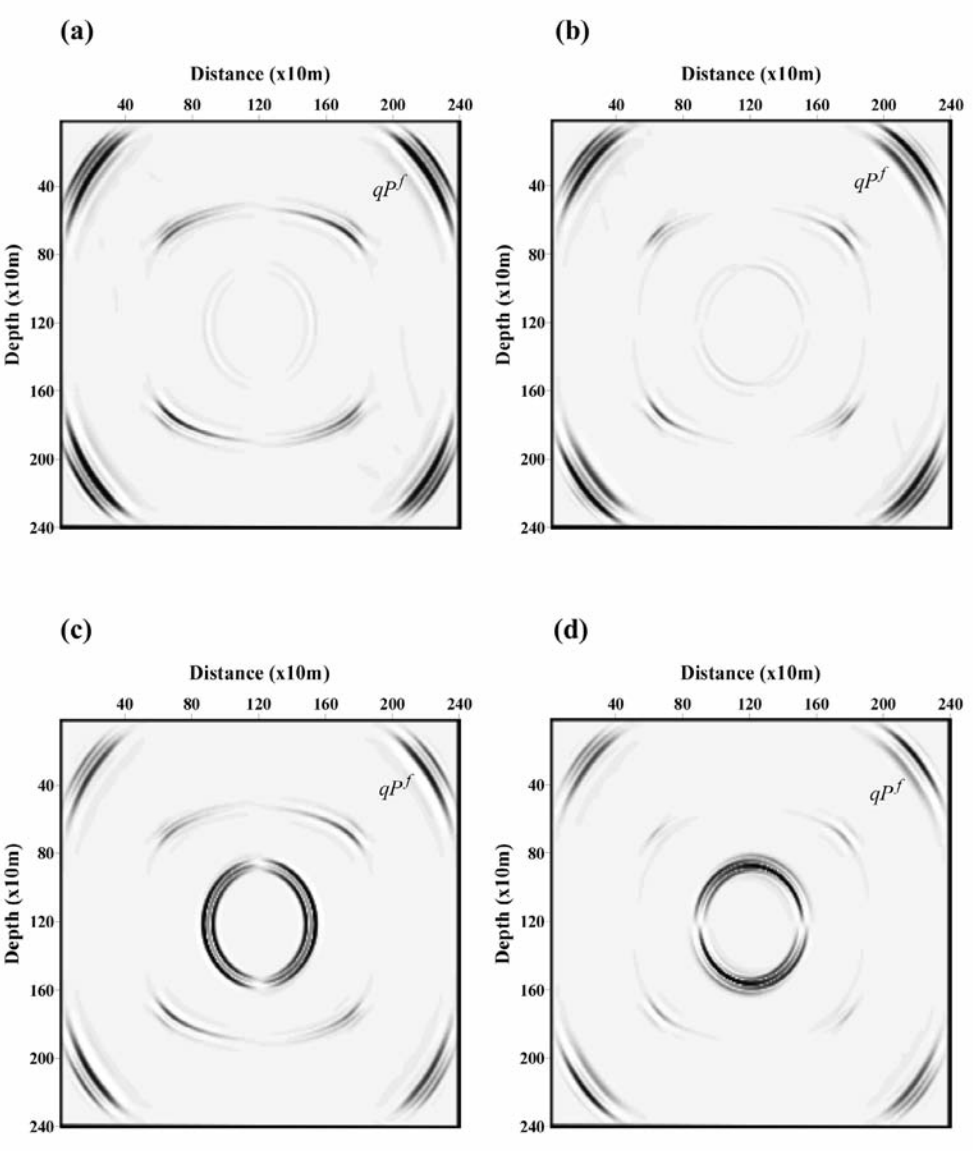

Fig. 5. Snapshots (t = 360 ms) of the horizontal (a,c) and vertical (b,d) components for the solid and fluid particle velocities based on BISQ mechanism with applying boundary conditions.

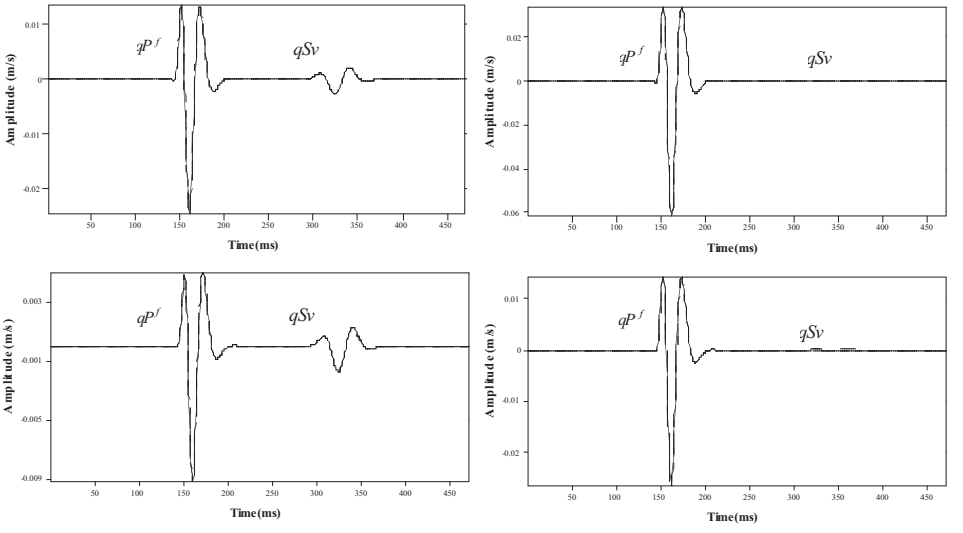

Fig. 6. The seismograms (the recording time is 470 ms) at the receiver position (60, 100). (a), (b), (c) and (d) show the horizontal and vertical components of the solid velocity and horizontal and vertical components of the fluid velocity, respectively. The solid lines indicate the exact solution, the dash lines indicate the numerical solution with C-PML, and the dotted lines represent the numerical solution with our nearly optimal boundary condition.

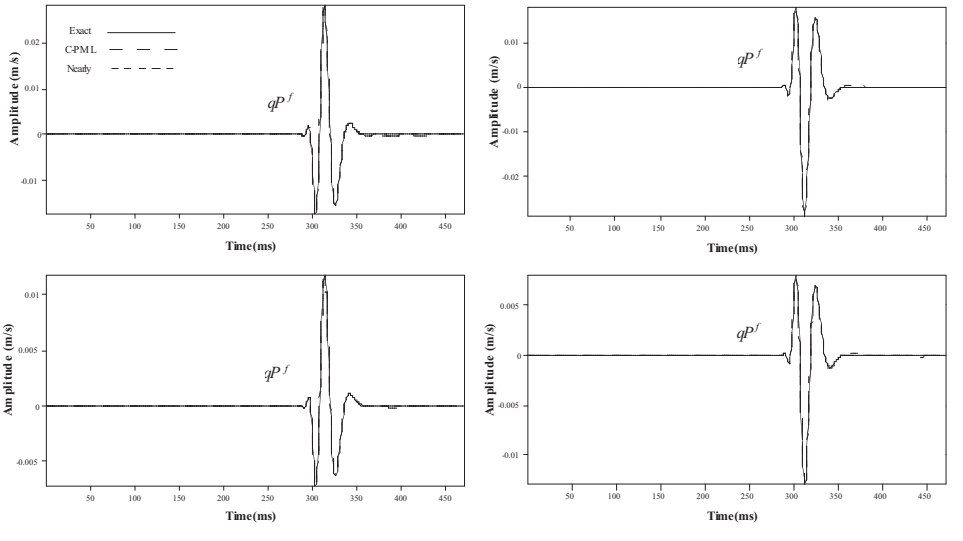

Fig. 7. The seismograms (the recording time is 470 ms) with the receiver grid (30,200). The details are the same as Fig. 6.

Fig. 7d shows the vertical component of the fluid velocity. In Figs. 6 and 7, the solid lines indicate the exact solution, the dashed lines indicate the numerical solution with C-PML, and the dotted lines represent the numerical solution with our nearly optimal boundary condition. All graphs show that our optimal boundary condition has the good performance as the C-PML does, and show that our nearly optimal boundary condition is an alternative effective tool. To showing the details, we separate the results into a, b, c, d in Fig. 8, using the horizontal component of the solid velocity at the position (30,200) as an example. Fig. 8a indicates the numerical solution without boundary condition, Fig. 8b indicates the exact solution, Fig. 8c indicates the numerical solution with C-PML, Fig. 8d indicates the numerical solution with our nearly optimal boundary condition. qP^fp indicates boundary reflections from qP^f.

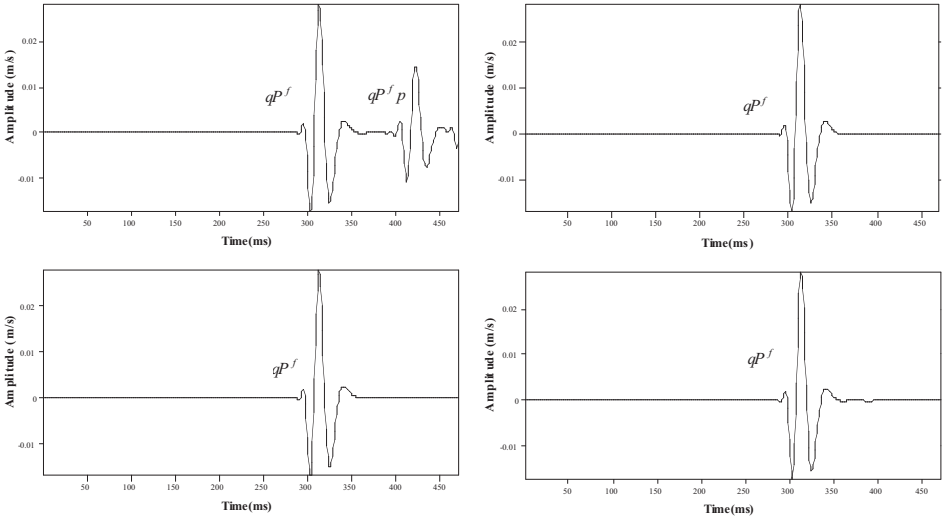

Fig. 8. The horizontal component of solid velocity at the position (30,200). (a), (b), (c) and (d) indicate the numerical solution without boundary condition, the exact solution, with C-PML, and with our nearly optimal boundary condition, respectively. qP^fp indicates boundary reflections from qP^f.

CONCLUSIONS

We present a modified nearly optimal sponge boundary condition. By minimizing energies of reflections from the boundaries across the model along x- and z-directions, respectively, we can find nearly optimal sponge length and absorbing coefficients. Finally, this method is applied to numerical simulation of seismic wave propagation in transversely isotropic poroelastic media based on Biot/squirt theory. The model test illustrates that this method can effectively eliminate the reflections from the edges of model.

ACKNOWLEDGMENTS

The authors would like to thank Atlantic Canada Opportunities Agency-AIF and Husky Energy for their generous support. The present work takes constructive suggestions from Dr. José Carcione that led to a significant improvement of the manuscript are gratefully acknowledged.

REFERENCES

Bérenger, J., 1994. A perfectly matched layer for the absorption of electromagnetic waves. J. Computat. Phys., 114: 185-200.

Biot, M.A., 1956a. Theory of propagation of elastic waves in a fluid saturated porous solid. I. Low-frequency rang. J. Acoust. Soc. Am., 28: 168-178.

Biot, M.A., 1956b. Theory of propagation of elastic waves in a fluid saturated porous solid. II. Higer-frequency range. J. Acoust. Soc. Am., 28: 179-191.

Biot, M.A., 1962. Mechanics of deformation and acoustic propagation in porous media. J. Appl. Phys., 33: 1482-1498.

Bording, R.P., 2004. Finite difference modeling-nearly optimal sponge boundary conditions. Expanded Abstr., 74th Ann. Internat. SEG Mtg., Denver: 1921-1924.

Carcione, J.M., 1996. Wave propagation in anisotropic, saturated porous media: plane wave theory and numerical simulation. J. Acoust. Soc. Am., 99: 2655-2666.

Carcione, J.M., 1998. Viscoelastic effective rheologies for modeling wave propagation in porous media. Geophys. Prosp., 46: 249-270.

Carcione, J.M., Helle, H.B. and Pham N.H., 2003. White's model for wave propagation in partially saturated rocks: Comparison with poroelastic numerical experiments. Geophysics, 68: 1389-1398.

Carcione, J.M. and Picotti, S., 2006. P-wave seismic attenuation by slow-wave diffusion: Effects of inhomogeneous rock properties. Geophysics, 71: O1-O8.

Carcione, J.M., 2007. Wave Fields in Real Media. Theory and numerical simulation of wave propagation in anisotropic, anelastic, porous and electromagnetic media. Elsevier Science Publishers, Amsterdam.

Cerjan, C., Kosloff, D., Kosloff, R. and Reshef, M. 1985. A nonreflecting boundary condition for discrete acoustic and elastic wave equations. Geophysics, 50: 705-708.

Clayton, R. and Engquist, B., 1977. Absorbing boundary conditions for acoustic and elastic wave equations. Bull. Seismol. Soc. Am., 67: 1529-1540.

Collino, F. and Monk, P., 1998. Optimizing the perfectly matched layer. Computer Meth. Appl. Mechanics Engineer., 164: 157-171.

Dai, N., Vafidis, A. and Kanasewich, E.R., 1995. Wave propagation in heterogeneous, porous media: A velocity-stress, finite-difference method. Geophysics, 60: 327-340.

Dong, L., She, D., Guan, L. and Ma, Z., 2005. An eigenvalue decomposition method to construct absorbing boundary conditions for acoustic and elastic wave equations. J. Geophys. Engineer., 2, 192-198.

Dvorkin, J. and Nur, A., 1993. Dynamic poroelasticity: A verified model with the squirt and the Biot mechanisms. Geophysics, 58: 523-533.

Dvorkin, J., Nolen-Hoeksema, R. and Nur, A., 1994. The squirt-flow mechanism: Macroscopic description. Geophysics, 59: 428-438.

Faria, E.L. and Stoffa, P.L., 1994. Finite-difference modeling in transversely isotropic media. Geophysics, 59: 282-289.

Graves, R.W., 1996. Simulating seismic wave propagation in 3d elastic media using staggered-grid finite difference. Bull. Seismol. Soc. Am., 86: 1091-1106.

Guddati, M.N. and Lim, K.W., 2006. Continued fraction absorbing boundary conditions for convex polygonal domains. Internat. J. Numer. Meth. Engin., 66: 949-977.

Hassanzadeh, S., 1991. Acoustic modeling in fluid saturated porous media. Geophysics 56, 424-435.

Higdon, R.L., 1991. Absorbing boundary conditions for elastic waves. Geophysics, 56: 231-241.

Komatitsch, D. and Martin, R., 2007. An unsplit convolutional perfectly matched layer improved at grazing incidence for the seismic wave equation. Geophysics, 72: SM155-SM167.

Kuzuoglu, M. and Mittra, R., 1996. Frequency dependence of the constitutive parameters of causal perfectly matched anisotropic absorbers. IEEE Microwave Guided Wave Lett., 6: 447-449.

Levander, A.R., 1988. Fourth-order finite-fifference P-SV seismograms. Geophysics, 53: 1425-1436.

Lou, M. and Rial, J.A., 1995. Modelling elastic-wave propagation in inhomogeneous anisotropic media by the pseudo-spectral method. Geophys. J. Internat., 120: 60-72.

Martin, R., Komatitsch, D. and Ezziani, A., 2008. An unsplit convolutional perfectly matched layer improved at grazing incidence for seismic wave propagation in poroelastic media. Geophysics, 73: T51-T61.

Mittet, R., 2002. Free-surface boundary conditions for elastic staggered-grid modeling schemes. Geophysics, 67: 1616-1623.

Moczo, P., Kristek, J. and Halada, L., 2000. 3D fourth-order staggered-grid finite-difference schemes: Stability and Grid dispersion. Bull. Seismol. Soc. Am., 90: 587-603.

Moczo, P., Kristek, J., Vavrycuk, V., Archuleta, R.J. and Halada, L., 2002. The heterogeneous staggered-grid finite-fifference modeling of seismic motion with volume harmonic and arithmetic averaging of elastic moduli and densities. Bull. Seismol. Soc. Am., 92: 3042-3066.

Mou, Y.G. and Pei, Z.L., 2005. Seismic Numerical Modeling for 3D Complex Media. Petroleum Industry Press, Beijing. ISBN 7-5021-4737-3.

Parra, J.O., 1997. The transversely isotropic poroelastic wave equation in cluding the Biot and the squirt mechanisms: Theory and application. Geophysics, 62: 309-318.

Pride, S.R., Berryman, J.G. and Harris, J.M., 2004. Seismic attenuation due to wave-induced flow. J. Geophys. Res., 109, B01201: 1-19.

Roden, J.A. and Gedney, S.D., 2000. Convolution PML (CPML): An efficient FDTD implementation of the CFS-PML for arbitrary media. Microwave Optic. Technol. Lett., 27: 334-339.

Sheen, D.H., Tuncay, K., Baag, C.E. and Ortoleva, P.J., 2006. Parallel implementation of a velocity-stress staggered-grid finite-difference method for 2-D poroelastic wave propagation. Computers & Geosci., 32: 1182-1191.

Sochacki, J., Kubichek, R., George, R., Fletcher, W.R. and Smithson, S., 1987. Absorbing boundary conditions and surface wave. Geophysics, 52: 60-71.

Quarteroni, A., Tagliani, A. and Zampieri, E., 1998. Generalized Galerkin approximations of elastic waves with absorbing boundary conditions. Computer Meth. Appl. Mechan. Engineer., 163: 323-341.

Thomsen, L., 1986. Weak elastic anisotropy. Geophysics, 51: 1954-1966.

Virieux, J., 1986. P-SV wave propagation in heterogeneous media: velocity-stress finite-difference method. Geophysics, 51: 889-901.

White, J.E., 1975. Computed seismic speeds and attenuation in rocks with partial gas saturation. Geophysics, 40: 224-232.

Yang, D.H. and Zhang, Z.J., 2000. Effects of the Biot and the squirt flow coupling interaction on anisotropic elastic waves. Chin. Sci. Bull., 45: 333-339.

Yang, D.H. and Zhang, Z.J., 2002. Poroelastic wave equation including the Biot/squirt mechanism and the solid/fluid coupling anisotropy. Wave Motion, 35: 223-245.

Zahradnik, J., Moczo, P. and Hron, F. 1993. Testing four elastic finite-difference schemes for behavior at discontinuities. Bull. Seismol. Soc. Am., 83: 107-129.

Zeng, Y.Q. and Liu, Q.H., 2001. A staggered-grid finite-difference method with perfectly matched layers for poroelastic wave equations. J. Acoust. Soc. Am., 109: 2571-2580.